Mine Water and the Environment (2022) 41:156–167
https://doi.org/10.1007/s10230-021-00820-z

TECHNICAL ARTICLE

Numerical Simulation of Mine Water Inflow with an Embedded Discrete Fracture Model: Application to the 16112 Working Face in the Binhu Coal Mine, China

Tao Chen[1] · Huiyong Yin[1] · Yutao Zhai[1] · Lin Xu[1] · Cuiyue Zhao[1] · Lifeng Zhang[2]

Received: 26 June 2020 / Accepted: 27 August 2021 / Published online: 18 January 2022

Abstract
Properly accounting for the effect of heterogeneity of aquifers and accurately predicting mine water inflow during the mining process is still a challenging problem in China. We developed a stochastic modelling methodology that considers a large range of possible multi-scale fracture configurations and heterogeneous porous rock to predict mine water inflow close to the observed data. The coupled discrete fracture–rock matrix models were built for the Binhu coal mine 16,112 working face with the Monte Carlo method. The models were solved using the embedded discrete fracture model to calculate groundwater inflow from the aquifer beneath the coal seam floor. The calculated results and the observed groundwater inflows in the field agreed well. Sensitivity analysis indicates that groundwater inflow increases with increased fracture length and fracture density. The effect of natural fractures introduces a large uncertainty for the models, due to the existence of long fractures that could act as conduits between the Ordovician limestone and no. 14 aquifers. The results highlight the importance of multi-scale fractures on modeling and simulating flow in the mine area.

Keywords Groundwater inflow · Coupled discrete fracture–rock matrix model · Monte Carlo method · Natural fractures · Mining-induced fracture · Heterogeneous porous media

Introduction

During deep underground coal mining, a series of environmental and ecological problems can arise due to alterations of the original hydraulic dynamics field and rock stress state of the area (Sun et al. 2015; Wu and Wang 2006; Yin et al. 2018; Zhang 2005), such as groundwater level depression (Zawadzki et al. 2016), groundwater pollution (Tiwary and Dhar 1994), land subsidence (Chen et al. 2016), and land desertification (Wang et al. 2008). Groundwater inrush into coal mines from aquifers underlying coal seams is a common problem, which influences the safety and poses a serious threat to the coal mine production (Guo et al. 2017; Yin et al. 2019). Therefore, accurately predicting and controlling groundwater inflow during coal mining is still a challenging problem.

Many analytical solutions (e,g. Hofedank and Engineers 1979; Marinelli and Niccoli 2000; Yihdego and Paffard 2017), numerical models (e.g. Azrag et al. 1998; Hernández et al. 2012), approximation models (e.g. Wu et al. 2011; Yoon et al. 2011; Bahrami et al. 2016), and experimental simulations (e.g. Zhang et al. 2017) have been developed to study groundwater inflow or inrush from below coal mine seam floors. It should be noted that while water inrush and inflow share some similarities in modelling methodology, an inrush is a sudden and catastrophic flow of water into the coal mines, often with danger to life and operations, an inflow is a steady and largely predictable volume that one is able to manage. Analytical solutions provide a simple and fast tool for calculating inflow into mines, but are generally unable to deal with models in complex hydrogeological situations. Instead, numerical methods are widely used for modeling groundwater inflow into coal mine due to their flexibility for dealing with hydrogeological heterogeneity and anisotropy, which

✉ Huiyong Yin
yhy1919@163.com

[1] Shandong Provincial Key Laboratory of Depositional Mineralization and Sedimentary Minerals, College of Earth Science and Engineering, Shandong University of Science and Technology, Qingdao 266590, China

[2] Binhu Coal Mine, Zaozhuang Mining (Group) Co., Ltd., Zaozhuang 277519, Shandong, China

requires greater computational effort. Approximation models such as artificial neural networks are powerful tools for solve groundwater problems that are capable of representing complex and non-linear processes. However, their performance largely depends on the selection of proper weight connections, network topology, and sufficient data during network training.

Dong et al. (2012) established a three-dimensional hydrogeological model of China's Linnancang Coal Mine to determine the characteristics of aquifers in the seepage field with FEFLOW and proved the necessity to pump water and simulate water levels under different boundary conditions. Zhu and Wei (2011) built a damage-based hydromechanical model and simulated mining-induced groundwater inrushes, considering the effect of faults and karst collapse columns with the finite element software, COMSOL. Yin et al. (2016) developed a numerical simulation model to study the evolution of flood water pathways under the Panxi longwall coal mine, China and discussed the characteristics of the failure depth of the coal seam floor. González-Quirós et al. (2019) built numerical flow models with the finite element method to evaluate the environmental risks during and after mine closure, based on an appropriate conceptualization of the mine-hydrogeological system. Such numerical models contribute to modeling water inrush into a coal mine by treating fractures as an equivalent porous medium in which the heterogeneity and anisotropy are not fully reflected, or as discretized unstructured grids, which are not feasible for use in large-scale geological models.

Many numerical models have been developed for fractured porous media (e.g. Chen et al. 2018; Huang et al. 2017; Jiang and Younis 2017), whereas few of these models have been applied in realistic scenarios, such as groundwater inflow into coal mines. We developed a novel stochastic modelling methodology that considers both multi-scale fractures and a heterogeneous rock matrix for dealing with more realistic geological scenarios. To characterize the complex geological structure of coal mines, a series of possible scenarios comprised of mining-induced fractures, natural fractures, and rock matrix is created using a Monte Carlo approach. These scenarios are solved numerically with the embedded discrete fracture model (EDFM) with Cartesian grids, which makes modeling large-scale geological models feasible compared to the unstructured grids associated with previous computational efforts. The proposed methodology provided a coal mine water inflow prediction close to the observed data. Sensitive analysis of fracture geometry on the mine water inflow was performed, which allows decision makers to quantify the uncertainty for groundwater inflow through the mine seam floors and to appropriately dewater to reduce the safety risk.

Conceptual Hydrogeological Model

The Binhu Coal Mine is located in Weishan, Shandong Province, China and the no. 161 West Mining District is located in northwest portion of the mine (Fig. 1a). The mining area is about 2.16 km wide from north to south, 2.99 km from east to west, and the mining area is 6.46 km^2 (Fig. 1b). The mining elevation ranges from − 500 m to − 760 m, and the thickness of the no. 16 coal, which belongs to the Taiyuan group, is 1.02–1.71 m, with an average of 1.25 m. Based on three-dimensional seismic exploration and coal roadway exposure, a total of 15 small and medium-sized faults near the mining area and boundary were identified. Except for two reverse faults, the rests are normal faults in the mining area. Because the main coal seam is relatively thin, the existence of faults influences the layout of the working face.

The 16,112 working face in the West Mining District (Fig. 1c,d) is 875–972 m long; the inclined length is about 204 m and the area is 164,880 m^2. The thickness is 1.1–1.6 m measured in boreholes, with an average of 1.3 m. The local section of the fault between the two faces of the working face exceeds 1.0 m. The coal seam structure is simple, the coal seam dip angle is 3°–12°, and the average is 7°. The immediate roof of the coal seam is the no. 10 L limestone, while the bottom is mudstone, generally with 0.6–1.0 m.

The main aquifers affecting the mining of the 16,112 working face are the immediate roof (the 10L Taiyuan group limestone), the no. 14 Benxi group limestone below the coal seam, and the Ordovician limestone aquifer. The 10 L limestone is a direct water-filled aquifer and the others are indirect water-filled aquifers (Fig. 2). In this study we focused on the water inflow from the floor, and whether the thick Ordovician limestone aquifer might threaten the safety of coal mining for the 16,112 working face. The 10L limestone is 3.7–4.1 m thick, with an average of 4.0 m. There are sandy mudstones, mudstone, coal, limestone, and fine sandstone between the no. 16 coal and no. 14 limestone, with an average thickness of 30.9 m. The no.14 limestone is about 22–28 m below the no. 16 coal seam, and has an average thickness of 11.5 m. The spacing between the no. 14 limestone and the Ordovician limestone ranges from 11.5 to 17.7 m, with an average of 14.7 m. The aquitard between these two limestones is mainly composed of clay mudstone and mudstone. The Ordovician limestone is about 59.6 m below the coal seam and is about 800 m thick. The rock matrix from the sandy mudstone beneath the no. 16 coal to the Ordovician limestone were considered the key strata for building conceptual models to investigate the water inflow from the 16,112 working face floor.

The mining-induced fracture zone consists of the immediate roof and bottom floor, and includes the

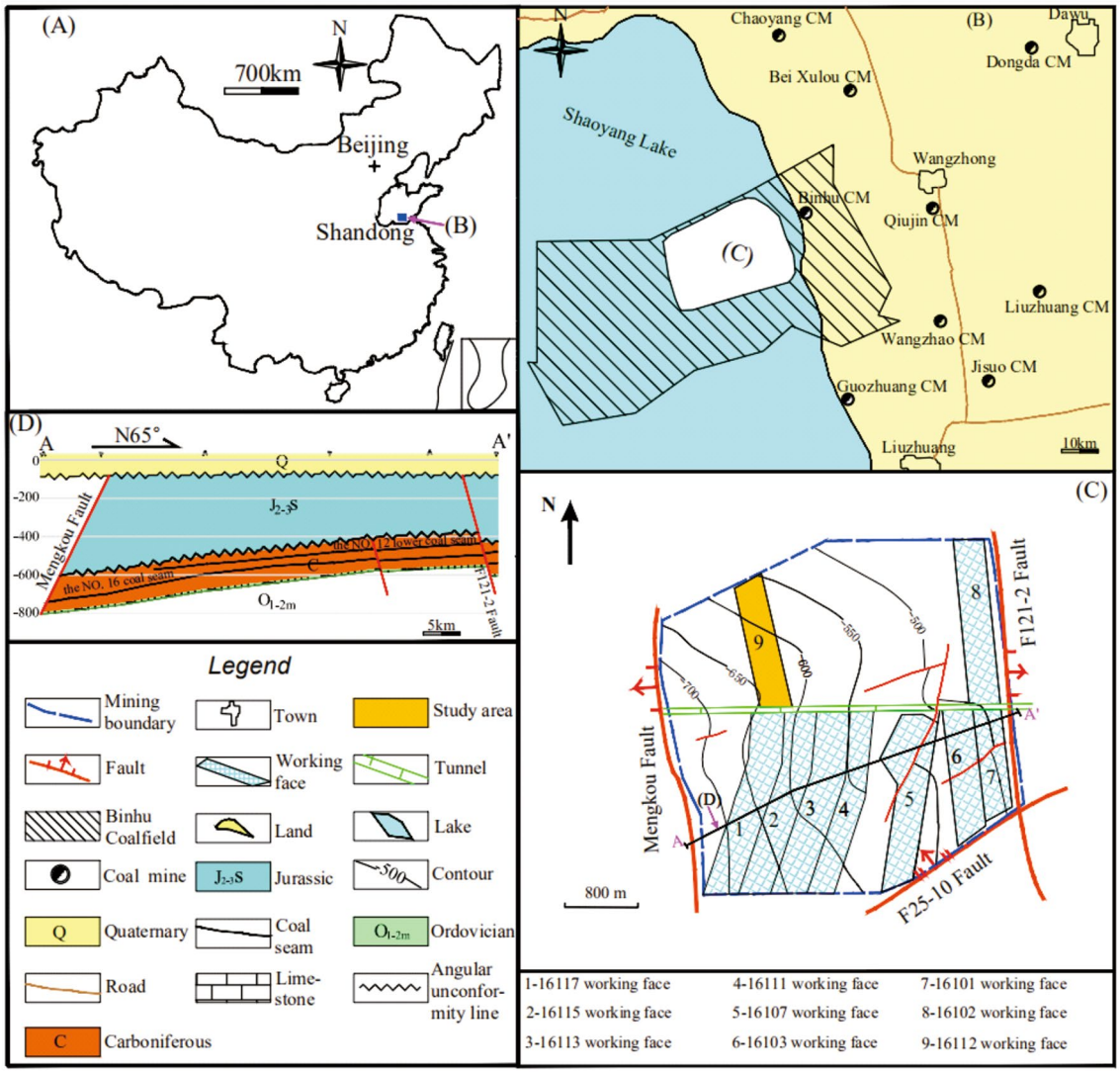

Fig. 1 **a** The location of Binhu Coal Mine, **b** the location of No.161 west mining district, and **c** the tectonic map and **d** the cross-section for No. 161 west mining district. The blue dashed lines represent the boundaries of the district and the red lines represent the main faults

water-conducting fracture zone, which can act as the main channel for water inrush from the immediate roof and bottom floor. The mining-induced fracture zone was estimated to extend 21–22 m beneath the floor of the 16,112 working face, based on empirical formulas.

The natural fracture zone refers to the fracture development zone caused by the structure, such as the fault, the associated fractures of the collapsed column, and the minor folding. The 16,112 working face has a monoclinic structure as a whole; the stress is concentrated, and the fractures tend to develop, near the axial plane of the folding in the 16,112 working face. This fracture zone can conduct water between the aquifers and the coal seam. Thus, natural fractures may have a great influence on the water filling of the no. 16 coal.

Numerical Flow Model Design

To account for the effect of fractures on mine water inflow through the floor of the 16,112 working face, we built a fractured porous rock model by incorporating discrete fractures into the heterogeneous rock matrix. Since the geological structure is relatively simple in the study area and there was no three-dimensional fracture geometric data, the fractures were represented as planar features. The model is simplified in two-dimensions. The discrete fractures include the mining-induced fractures and natural fractures (Fig. 3a). The rock matrix includes both aquifers and aquicludes (Fig. 3b). The dimensions of the model are 100 m × 100 m in the x–z plane. The mining-induced

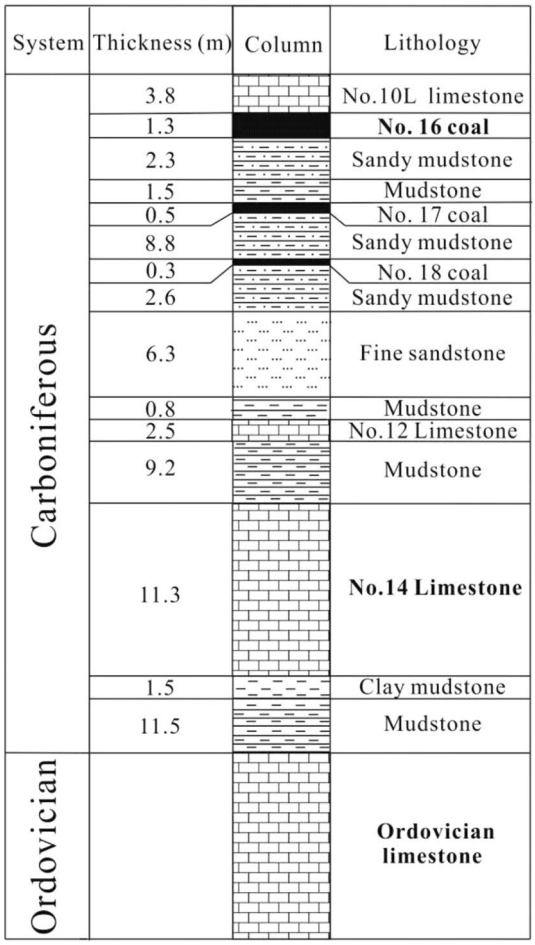

Fig. 2 Stratigraphic column of the 16,112 working face

fractures below the floor are distributed within about 22 m of the coal seam, based on experience for the 16,112 working face. The natural fractures were assumed to be distributed to depths of 20–60 m below the mine floor. After determining the fracture locations in the domain, the orientation and length of the fractures were defined for each fracture, as listed in Table 1. The fracture orientation was assumed as a Fisher distribution, according to the statistical analysis of field measurement data in the fields (e.g. Gutierrez and Youn 2015). Both mining-induced fractures and natural fractures were generated stochastically based on ADFNE code (Alghalandis 2017) and integrated into the model. The apertures for the fractures were assumed to be 1×10^{-4} m and the hydraulic aperture was assumed to be 8×10^{-5} m, due to the roughness of the fracture surface, which is comparable to measured data (e.g. Hakami and Larsson 1996). The permeability of fractures is 5.33×10^{-10} m^2 (equivalent to a hydraulic conductivity of 451 m/day), according to cubic law.

For the rock matrix, the no. 14 and Ordovician limestones are assumed to be aquifers. The no. 14 limestone, which ranges from 25 to 37 m in depth, has a hydraulic conductivity of 0.0065 m/day, according to pumping tests. The Ordovician limestone extends from 60 to 100 m in depth below the coal seam, with a hydraulic conductivity of 0.19 m/day, according to pumping tests. We should note that in-situ pumping test measurements provides a more reliable estimation for hydraulic properties at the field scale than laboratory measurements of rock samples, as discussed by Neuman (2005). The rock matrix intervals among the 16,112 working face and these two limestones were assumed to be aquicludes with a hydraulic conductivity of 8.64×10^{-5} m/day (e.g. Timms et al. 2014).

The groundwater inflow in the bottom portion of the 16,112 working face ranged from the initial 25 m^3/h to a maximum of 28 m^3/h from Feb. 26, 2019 to March 6, 2019, which was relatively minor and stable. Given the large volume of the Ordovician limestone, we assumed

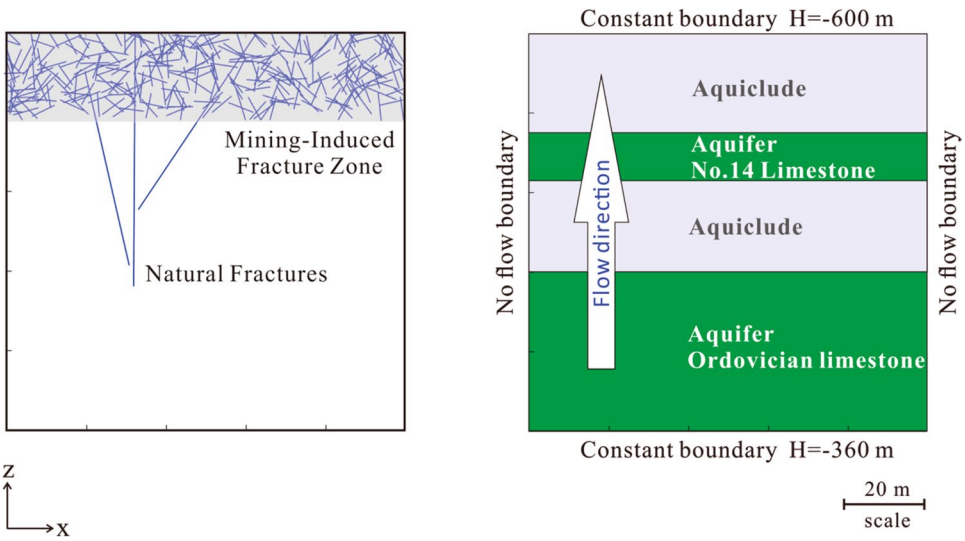

Fig. 3 **a** Discrete fracture system and **b** rock matrix system and boundary conditions for the numerical model

Table 1 Geometric properties for generating stochastic fractures

Fracture network geometry		Mining-induced fractures	Natural fractures
Fracture length	Distribution type	Exponential	Exponential
	Mean	8	60
Fracture orientation	Distribution type	Random	Fisher
	Mean	–	90
	Kappa	–	8
Fracture number		300	3

that these inflows were mainly from the Ordovician limestone. As the period of the study was short (about 8 days) and the water inflow rate was low, hydraulic head variations could be neglected, since there was an infinite source of water at a small temporal and spatial scale. Furthermore, we neglected horizontal variations in the model's boundary condition and rock properties, and simplified it as a two-dimensional model. Accordingly, the observed water inflow tended to be steady-state with a volume of 25–28 m^3/h on the bottom portion (the top boundary of the model). The model's lateral boundaries were defined as no-flow boundaries, as we assumed that the hydraulic gradient in the z-direction dominates the groundwater flow field (Fig. 3b). The top boundary was assigned a constant hydraulic head of − 600 m, according to the evacuation depth to the working surface. The bottom boundary was assumed to be a constant hydraulic head of − 360 m according to borehole observation data for the Ordovician limestone.

Embedded Discrete Fracture Model

For fractured porous media, which includes both fractures and rock matrix, the rock matrix can be represented by a two- or three-dimensional grid. Fractures are then explicitly represented with a lower one- or two-dimensional grid, due to their extremely small apertures compared to the matrix block dimensions in the numerical model (Fig. 4). The discrete fracture and the rock matrix are coupled with an embedded fracture modeling approach (Hajibeygi et al. 2011; Li and Lee 2008; Moinfar et al. 2012).

For embedded discrete fracture models, the mass conservation equation for the rock matrix and fracture can be expressed as:

$$S_s{}^m \frac{\partial h^m}{\partial t} = \nabla \bullet \left[K^m(\nabla h^m)\right] + Q^m - \psi^{mf}, \tag{1}$$

and

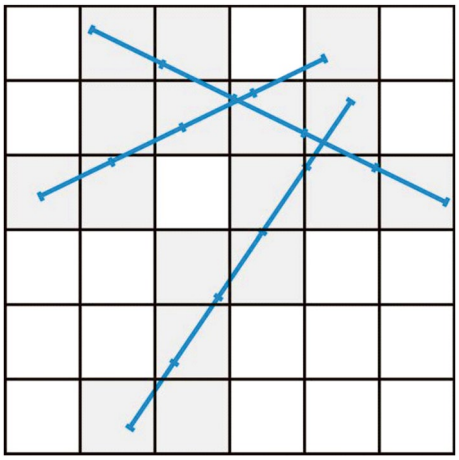

Fig. 4 Embedded discrete fracture model. The 2D black grid represents rock matrix, the 1D blue grid represent fracture, and the grey grid represents the rock matrix that coupling with fractures

$$S_s{}^f \frac{\partial h^f}{\partial t} = \nabla \bullet \left[K^f \left(\nabla h^f\right)\right] + Q^f - \psi^{fm}, \tag{2}$$

respectively, where S_s, h, t, K, and Q represent specific storage, hydraulic head, time, hydraulic conductivity, and source or sink term, respectively. Superscripts m and f represent matrix and fracture quantities, respectively. The mass exchange between fracture and matrix grid, ψ^{mf} and ψ^{fm}, are expressed as:

$$\psi^{mf} = CI \bullet K^m \left(h^m - h^f\right) = -\psi^{fm}, \tag{3}$$

where CI is the fracture-matrix conductivity index. Interaction of a matrix grid block i and a fracture grid element j is defined as:

$$CI = \frac{A_{i-j}}{\langle d \rangle_{i-j}}, \tag{4}$$

where A_{i-j} is the plane area of fracture grid element i inside the matrix grid block j, and $\rangle d\rangle_{i-j}$ is the average distance between matrix grid block i and fracture grid element j, which can be expressed as:

$$\langle d \rangle_{i-j} = \frac{\int_V x_n dv}{V}, \tag{5}$$

where dv, x_n and V are the volume element, the normal distance of the element from the fracture, and the volume of a rock matrix grid block, respectively.

An advantage of EDFM is that the fracture and matrix grids are independent and, thus, suited for many realistic scenarios such as naturally fractured reservoirs and dynamic fracture generation and closures. The equation is discretized by a finite volume method and can be

implemented within the framework of open-source Matlab simulator MRST code (Lie et al. 2012).

Numerical Results

We build one hundred stochastic discrete fracture–rock matrix models with the fracture geometric parameters listed in Table 1. Some of the possible fracture configurations are shown in Fig. 5. The mining-induced fractures were distributed relative evenly within the depth of 22 m. Due to the high uncertainty of the natural fractures, the positions of natural fractures were distributed more randomly. They are nearly above the Ordovician limestone aquifer (realizations #1, #7, and #9 in Fig. 5) or penetrate the Ordovician limestone and the no. 14 limestone aquifer as conduits (realizations #5, #8, and #10 in Fig. 5). The complexity of the heterogeneity can be represented intuitively by the coupled discrete fracture–rock matrix geological models.

The mine water inflow problem was solved by the embedded discrete fracture model for the stochastically generated discrete fracture–rock matrix models shown above. The dimensions of the rock matrix grid are 1 m × 1 m and the dimension of the fracture grid is 2.5 m. The hydraulic head for the steady-state flow models is shown in Fig. 6. They show the hydraulic head distributions that would intuitively be expected for various fracture–rock matrix configurations. For the aquifer zones of the no. 14 and Ordovician limestones, the hydraulic head tends to be to uniform. For the aquiclude zone between the two limestones, the hydraulic head changes gradually. However, the hydraulic head of the model is highly influenced by the presence of the fractures. For the aquiclude zone beneath the 16,112 working face, a relatively uniform hydraulic head zone within 22 m in depth (the depth of the mining-induced fractures extends) due to the highly permeable mining fractures observed. Such characteristics are altered by the existence of natural fractures. If the natural fractures do not fully act as a conduit between the no. 14 and Ordovician limestone aquifers (realizations

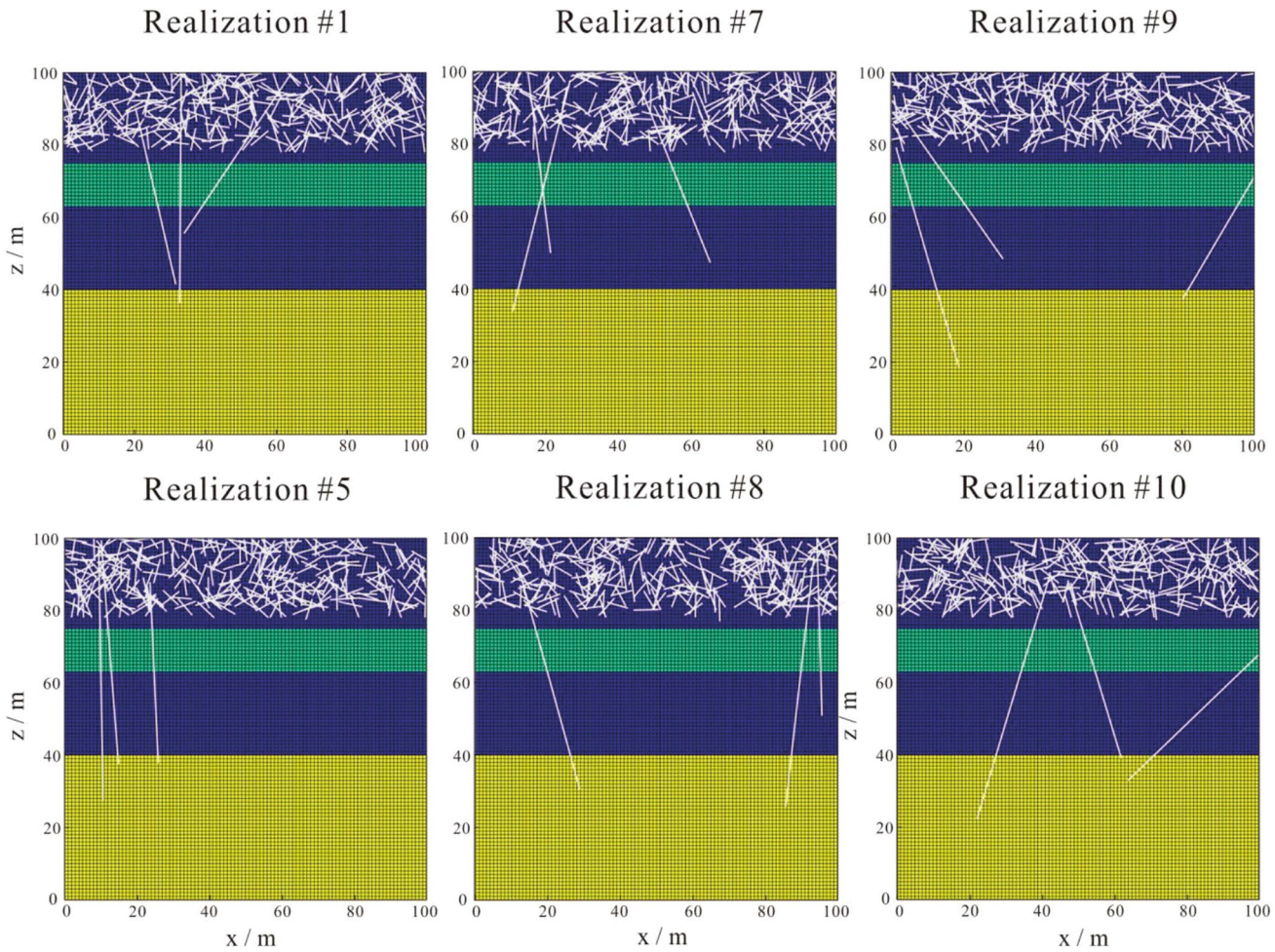

Fig. 5 Realizations of the coupled discrete fracture–rock matrix model

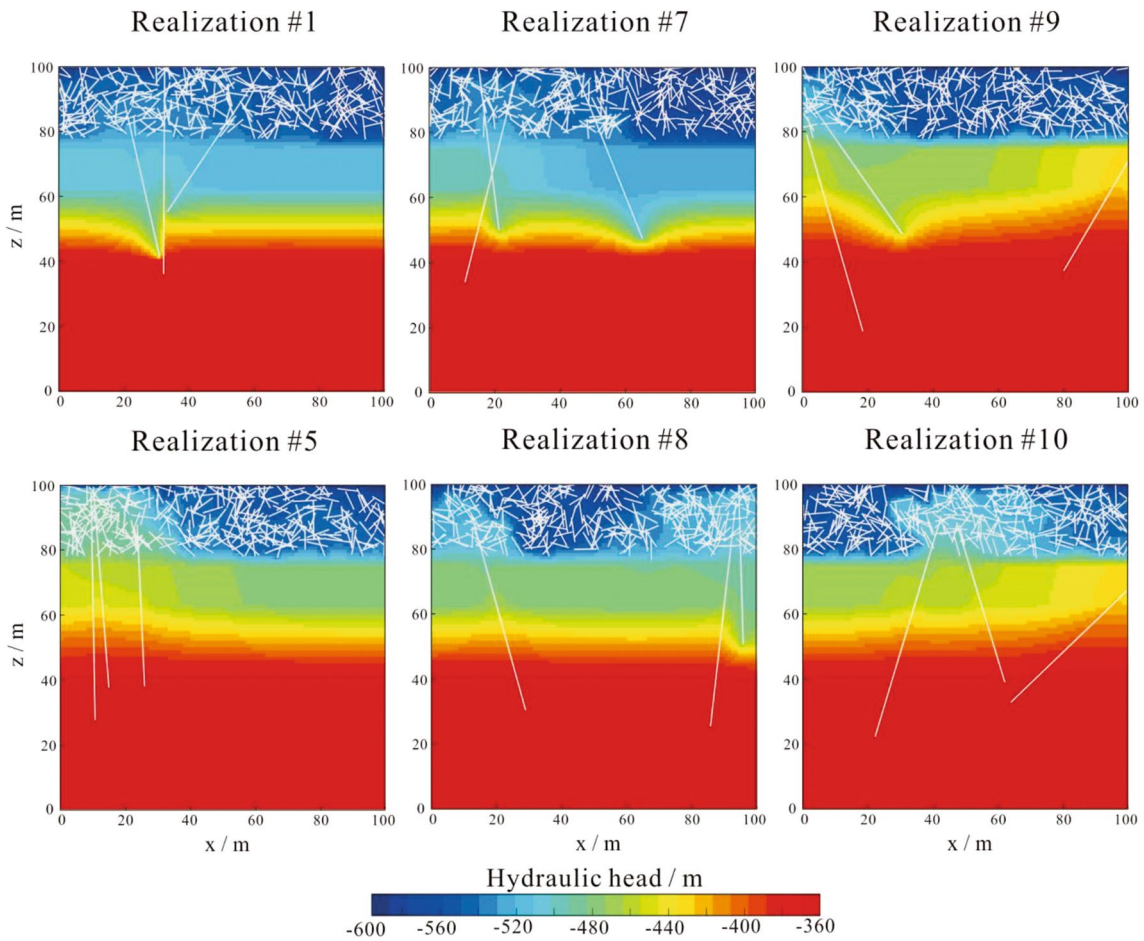

Fig. 6 Hydraulic head of the realizations of the coupled discrete fracture–rock matrix model

#1, #7, and #9 in Fig. 5), the alteration is relatively small, whereas in realizations #5, #8, #10, more fractures penetrate the aquifers and a relatively high hydraulic head zone is observed in the mining fracture-aquiclude zone.

We computed the groundwater flow rate on the top boundary of the model, which stands for the inflow of mine water at the 16,112 working face. The flow rate on the whole top boundary of the model is divided by its length and yields the inflow of mine water per m^2. The calculated groundwater inflow of the coal mine seam floor ranges from 4.3×10^{-5} to 2.6×10^{-4} m^3/h per unit area, with an average of 1.6×10^{-4} m^3/h. The observed groundwater inflow for the 16,112 working face is 25–28 m^3/h, which is measured by flowmeter in a drainage ditch. Considering the area of the 16,112 working face of 164,880 m^2, the observed inflow of mine water is 1.5×10^{-4} to 1.7×10^{-4} m^3/h per unit area. It shows that the difference between the calculated and the measured groundwater inflow is very small which suggests that the modelling method produces expected results and a realistic range of inflows. Furthermore, realizations #5, #8, #10 have a higher groundwater inflow than the other realizations. This is mainly due to the existence of natural fractures, which connect the no. 14 and Ordovician limestone aquifers, resulting in a high hydraulic head in the mining fracture zone. For comparison, we calculated the groundwater inflow for the conceptual models for the rock matrix (aquifers and aquiclude), with mining-induced fractures and with natural fractures (Fig. 7). It shows that compared to the mining-induced fractures, the natural fractures have a greater impact on groundwater inflow and introduce a bigger uncertainty. The groundwater inflow increased sharply when the rock matrix, mine-induced fractures, and natural fractures were coupled, which is accompanied by greater uncertainty. Overall, it shows that the modelling method yields a realistic prediction of water inflows.

Furthermore, based on the water outflow on the top boundary, we also calculated the equivalent hydraulic conductivity *K*eq of the discrete fracture–rock matrix system for the realizations, which ranges from 4.4×10^{-4} to 2.6×10^{-3} m/day. The equivalent hydraulic conductivity for the discrete fracture–rock matrix system, which is larger than that of the aquiclude, is reasonable, since the fractures

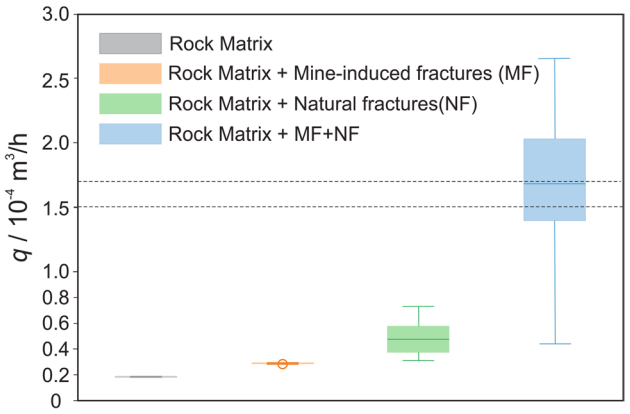

Fig. 7 Box plot of the calculated groundwater inflow per unit area for the realizations. The dashed black lines represent the measured groundwater inflow at the 16,112 mine working face

may cross the aquiclude and connect the mining-induced fracture zones and aquifers.

Sensitivity Analysis

We also did a series of sensitivity analysis for the mine water inflow for both the mining-induced fractures and natural fracture geometries. Herein, the fracture length and the number of fractures (fracture density) are considered. For the mining fractures, the number of fractures were varied from 100, to 200, 300, 400, and 500. Ten stochastic realizations of the discrete fracture–rock matrix model were generated for each fracture geometric parameter. The groundwater inflow for the models is shown in Fig. 8. It shows that the groundwater inflow increased with the fracture number, from 3.5×10^{-5} to 2.6×10^{-4} m^3/h (Fig. 8a). A sensitivity analysis for the average mining fracture length was also performed, varying it from 4, to 6, 8, 10, and 12 m (Fig. 8b). The groundwater inflow increased with the fracture number, from 3.6×10^{-5} to 2.7×10^{-4} m^3/h. It is reasonable that increases of fracture number and length for the mining-induced fractures results in a more permeable zone and increases the mine water inflow. It is interesting to note that when the fracture number or fracture length was small (100 and 200 for fracture number or 4 m and 6 m for mining fracture length), the uncertainty of inflow was relatively small with a narrow range. When they increased, the groundwater inflow had a wider range, which indicates that the uncertainty of the results increases. With respect to the considerably high hydraulic conductivity of the fractures compared with the limestone, an increase in number and length would result in greater contact and therefore increased water inflow. If all of the fractures in the model were closely spaced (i.e. small aperture), then the flow could be less than if they are widely spaced (i.e. large aperture), as at some point the hydraulic

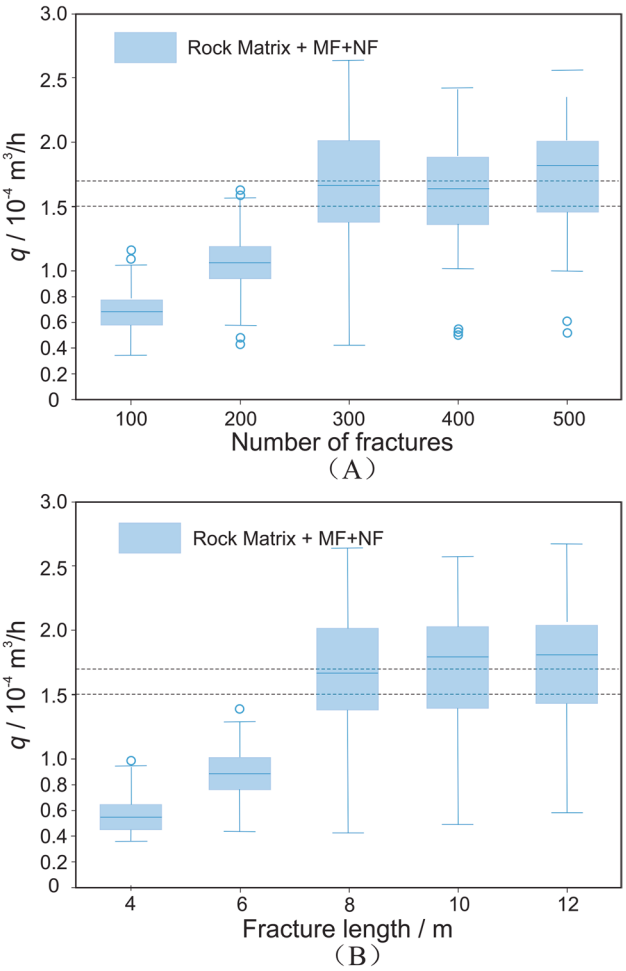

Fig. 8 Box plot of the calculated groundwater inflow per unit area **a** for varied fracture numbers and **b** for varied fracture length regarding mining-induced fractures. The dashed black lines represent the measured groundwater inflow

properties of the limestone become more important than those of the fractures.

A similar sensitivity analysis was performed for the natural long fracture set. The number of fractures (fracture density) ranged from 1, 2, 3, 4, to 5 and the average length of the fractures changed from 30, to 45, 60, 75, and 90 m. Again, ten stochastic models were generated for each parameter set. The changes of groundwater inflow are shown in Fig. 9a,b, which also shows that the groundwater inflow per unit area of the working face increased both with the fracture number and fracture density over a similar range, from 2.9×10^{-5} to 2.8×10^{-4} m^3/h. It is interesting to note that there is a big uncertainty when the fracture number is 2 and a low uncertainty when the fracture number is 4 (Fig. 9a). By contrast, when the fracture length increases, the uncertainty of the models does not exhibit a clear variation (Fig. 9b).

This sensitivity analysis shows the results that might be expected given the conceptual hydrogeological model where

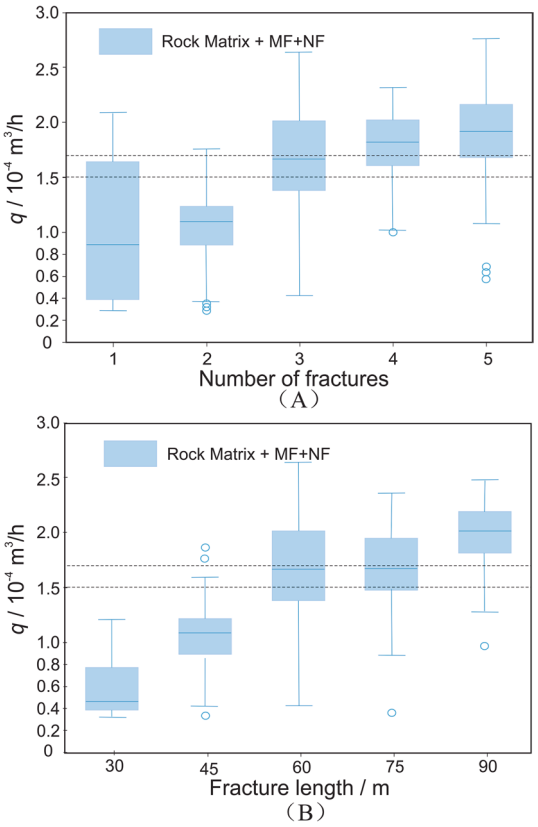

Fig. 9 Box plot of the calculated groundwater inflow per unit area **a** for varied fracture numbers and **b** for varied fracture length regarding natural fractures. The dashed black lines represent the measured groundwater inflow

water is largely derived from the basal Ordovician limestone via long connecting natural fractures to the mining-induced fractured horizon and the mine floor. If the mine-induced fracture system is more permeable, then it will transport more coal mine water away from those deep fractures. The 'uncertainty' shown in the spread of each box plot is largely the result of the (variable) distribution of the natural long fractures in the models. Furthermore, the increase of calculated groundwater inflow with the fracture geometries can be roughly classified into two stages. For example, when the length of natural fractures was less than 60 m, we assumed that they did not interconnect the Ordovician limestone with the mining-induced fractured horizons. Thus, the calculated groundwater inflow increase obviously with fracture length. Once the two horizons were connected by fractures longer than 60 m, then the calculated groundwater inflow increased mildly and then stabilized (Fig. 9b). Figure 9a tends to support the same argument. Lastly, we conducted a statistical analysis considering all of the possible model results shown above. It showed that the mean inflow was 1.18×10^{-4} m^3/h, with upper and lower bounds of 1.76×10^{-5} m^3/h and 1.99×10^{-4} m^3/h, respectively.

Discussion and Conclusions

In this study, a series of stochastic discrete fracture–rock matrix systems were built for the 16,112 working face. The rock matrix includes aquifers and aquicludes and the fractures include both mining-induced and natural fractures. This led to an innovative methodology for building coupled discrete fracture–rock matrix hydrogeological conceptual models. The groundwater inflow was solved using embedded discrete fracture models, which improved the computational efficiency of the numerical models. This novel methodology provided a realistic estimate of mine water inflow where we have limited data. The uncertainty of the stochastically generated models was also analyzed. The proposed methodology helps in modeling groundwater inflow into coal mines regarding the effect of multi-scale fractures, which should be useful to decision makers attempting to reduce the risk of inrush problems.

We should note that the embedded discrete fracture models are based on non-conforming meshes for fracture–rock matrix systems, which reduced the computational efforts. The embedded discrete fracture models yielded accurate results in a simpler configuration than semi-analytical results (Shakiba 2014). They may have a slightly higher error of pressure or hydraulic head compared with other discrete fracture models with conforming meshing for complex configurations (Flemisch et al. 2017). The embedded discrete fracture models have been improved recently to consider multiphase flow (Jiang and Younis 2017), the mechanical effect of fractures (Norbeck et al. 2015), and for analysis of fractured wells with complex fractures geometries (Liu et al. 2021). Nevertheless, they are rarely combined with stochastically generated multi-scale fracture–rock matrix systems and applied in coal mine water inflow prediction. In this work, we developed a stochastic methodology for including multi-scale fracture and heterogeneous rock matrix in two dimensions. The proposed workflow yielded a realistic prediction of water inflows in the Binhu coal mine, which suggests that the proposed methodology might be extended to deal with more complex hydrogeological scenarios requiring the use of three-dimensional models. Additionally, the methodology could be extended for two-phase flow water inrush hazard (e.g. Ma et al. 2020) and fault activity (e.g. Zhou et al. 2017) in coal mine areas.

Compared to the equivalent fracture model, the proposed discrete fracture–rock matrix model explicitly considers the geometry of fractures (Berkowitz 2002). Furthermore, the embedded discrete fracture model requires less meshing effort than other discrete fracture models (Li and Lee 2008; Moinfar 2012). However, there were three major limitations in this study:

- First, the proposed methodology requires detailed fracture geometric data compared to equivalent fracture models, in which the bulk hydraulic properties of fractured rocks are estimated by pumping tests. Thus, multi-scale fracture characterization data, both for mining-induced and natural fractures (e.g. Mao et al. 2018; Wang et al. 2017), is required to further reduce the uncertainty the models. While we generated a series of discrete fracture–rock matrix scenarios with stochastic methodology, inflow rates will clearly depend on many factors, such as fracture frequency, hydraulic aperture, and source aquifer characteristics. These uncertainties need to be reviewed carefully in further study. Furthermore, the relationship between the fracture position and the layered rock matrix, which may influence the distribution of natural fractures (e.g. Gale et al. 2014), should be explored for improved understanding of the conceptual model.
- Second, considering the relatively short time period and the small changes in the measured inflow, the flow was assumed to be steady-state in this study, which indicates that the inflow and hydraulic head are time-independent in the model. However, for a long-period prediction, long-time groundwater flow monitoring data is necessary to build transient models that consider seasonal components and to calibrate the models.
- Third, the two-dimensional model built in this study was appropriate for the relatively simple geological setting and the availability of the fracture geometric data. The model should eventually be extended to three dimensions with more characterization data, though this will greatly increase the complexity of the models. As a compromise, small and intense fractures can be created stochastically and be represented by equivalent hydraulic properties with upscaling methods, while large fractures can be represented explicitly in the model (Chen et al. 2018; Li and Lee 2008). Although applied here in two dimensions, this study highlights the importance of considering the geometries of multi-scale discrete fractures in simulating groundwater inflow into coal mines.

To summarize, regarding the multi-scale fracture sets and the heterogeneous rock matrix in realistic geological models, a stochastic methodology was developed based on the Monte Carlo method and the embedded discrete model for predicting realistic groundwater inflow and for making dewater measurements for coal mine seam floors. The following major conclusions can be drawn from our study:

(1) Groundwater inflow is controlled both by the distributions of the aquifers and the geometry of the fractures. Even before the Ordovician limestone and mining-induced fracture horizons are connected, the calculated groundwater inflow increased greatly with the length and the number of fractures. Once the two horizons were connected by natural fractures, the inflow increased slowly with the fracture geometries.

(2) The groundwater inflow increased with the fracture density and number of fractures. For the mining-induced fractures, lower density and shorter length resulted in less uncertainty. For the natural fractures, the number of fractures produced more uncertainty than the length of the fractures.

Acknowledgements We thank the editors and the three anonymous reviewers for their constructive feedback and insightful comments which greatly improved this paper. The research was financially supported by the: National Key R&D Program of China 2017YFC0804101), National Natural Science Foundation of China (42002261), National Natural Science Foundation of Shandong Province (ZR2019MD013; ZR2019BD028), Science and Technology Research Guiding Program, China National Coal Association (MTKJ 2018-262), and Scientific Research Foundation of Shandong University of Science and Technology for Recruited Talents (2019RCJJ004). The authors are grateful to the developers of the open source code ADFNE and MRST.

References

Alghalandis YF (2017) ADFNE: open source software for discrete fracture network engineering, two and three dimensional applications. Comput Geosci 102:1–11. https://doi.org/10.1016/j.cageo.2017.02.002

Azrag EA, Ugorets VI, Atkinson LC (1998) Use of a finite element code to model complex mine water problems. Proc Int Mine Water Assoc Symp Mine Water Environ Impacts (johannesburg, South Africa) 1:31–41

Bahrami S, Ardejani FD, Baafi E (2016) Application of artificial neural network coupled with genetic algorithm and simulated annealing to solve groundwater inflow problem to an advancing open pit mine. J Hydrol 536:471–484. https://doi.org/10.1016/j.jhydrol.2016.03.002

Berkowitz B (2002) Characterizing flow and transport in fractured geological media: a review. Adv Water Resour 25(8–12):861–884. https://doi.org/10.1016/S0309-1708(02)00042-8

Chen SJ, Yin DW, Cao FW, Liu Y, Ren KQ (2016) An overview of integrated surface subsidence-reducing technology in mining areas of China. Nat Hazards 81(2):1129–1145. https://doi.org/10.1007/s11069-015-2123-x

Chen T, Clauser C, Marquart G, Willbrand K, Hiller T (2018) Upscaling permeability for three-dimensional fractured porous rocks with the multiple boundary method. Hydrogeol J 26(6):1903–1916. https://doi.org/10.1007/s10040-018-1744-z

Dong D, Sun W, Xi S (2012) Optimization of mine drainage capacity using FEFLOW for the no 14 coal seam of China's Linnancang coal mine. Mine Water Environ 31(4):353–360. https://doi.org/10.1007/s10230-012-0205-5

Flemisch B, Berre I, Boon W, Fumagalli A, Schwenck N, Scotti A, Stefansson I, Tatomir A (2018) Benchmarks for single-phase flow in fractured porous media. Adv Water Resour 111:239–258. https://doi.org/10.1016/j.advwatres.2017.10.036

Gale JF, Laubach SE, Olson JE, Eichhubl P, Fall A (2014) Natural fractures in shale: a review and new observations. AAPG Bull 98(11):2165–2216. https://doi.org/10.1306/08121413151

González-Quirós A, Fernández-Álvarez JP (2019) Conceptualization and finite element groundwater flow modeling of a flooded underground mine reservoir in the Asturian Coal Basin. Spain J Hydrol 578:124036. https://doi.org/10.1016/j.jhydrol.2019.124036

Guo WJ, Zhao JH, Yin LM, Kong DZ (2017) Simulating research on pressure distribution of floor pore water based on fluid-solid coupling. Arab J Geosci 10(1):5. https://doi.org/10.1007/s12517-016-2770-6

Gutierrez M, Youn DJ (2015) Effects of fracture distribution and length scale on the equivalent continuum elastic compliance of fractured rock masses. J Rock Mech Geotech 7(6):626–637. https://doi.org/10.1016/j.jrmge.2015.07.006

Hajibeygi H, Karvounis D, Jenny P (2011) A hierarchical fracture model for the iterative multiscale finite volume method. J Comput Phys 230(24):8729–8743. https://doi.org/10.1016/j.jcp.2011.08.021

Hakami E, Larsson E (1996) Aperture measurements and flow experiments on a single natural fracture. Int J Rock Mech Min 33(4):395–404. https://doi.org/10.1016/0148-9062(95)00070-4

Hernández JH, Padilla F, Juncosa R, Vellando PR, Fernández Á (2012) A numerical solution to integrated water flows: application to the flooding of an open pit mine at the Barcés river catchment–La Coruña, Spain. J Hydrol 472:328–339. https://doi.org/10.1016/j.jhydrol.2012.09.040

Hofedank RH, Engineers OGC (1979) Computation of and experience on lignite opencast mine drainage. In: Proceedings of the 1st international mine drainage symposium, Denver, Colorado, pp 383–408

Huang N, Jiang YJ, Liu RC, Li B (2017) Estimation of permeability of 3-D discrete fracture networks: an alternative possibility based on trace map analysis. Eng Geol 226:12–19. https://doi.org/10.1016/j.enggeo.2017.05.005

Jiang J, Younis RM (2017) An improved projection-based embedded discrete fracture model (pedfm) for multiphase flow in fractured reservoirs. Adv Water Resour 109:267–289. https://doi.org/10.1016/j.advwatres.2017.09.017

Li L, Lee SH (2008) Efficient field-scale simulation of black oil in a naturally fractured reservoir through discrete fracture networks and homogenized media. SPE Reserv Eval Eng 11(04):750–758. https://doi.org/10.2118/103901-PA

Lie KA, Krogstad S, Ligaarden IS, Natvig JR, Nilsen HM, Skaflestad B (2012) Open-source MATLAB implementation of consistent discretisations on complex grids. Comput Geosci 16(2):297–322. https://doi.org/10.1007/s10596-011-9244-4

Liu H, Liao X, Tang X, Chen Z, Zhao X, Zou J (2021) A well test model based on embedded discrete-fracture method for pressure-transient analysis of fractured wells with complex fracture networks. J Petrol Sci Eng 196:108042. https://doi.org/10.1016/j.petrol.2020.108042

Ma D, Duan H, Liu W, Ma X, Tao M (2020) Water–sediment two-phase flow inrush hazard in rock fractures of overburden strata during coal mining. Mine Water Environ 39:308–319. https://doi.org/10.1007/s10230-020-00687-6

Mao D, Liu Z, Wang W, Li S, Gao Y, Xu Z, Zhang C (2018) An application of hydraulic tomography to a deep coal mine: combining traditional pumping tests with water inrush incidents. J Hydrol 567:1–11. https://doi.org/10.1016/j.jhydrol.2018.09.058

Marinelli F, Niccoli WL (2000) Simple analytical equations for estimating ground water inflow to a mine pit. Groundwater 38(2):311–314. https://doi.org/10.1111/j.1745-6584.2000.tb00342.x

Moinfar A, Varavei A, Sepehrnoori K, Johns RT (2012) Development of a novel and computationally-efficient discrete-fracture model to study IOR processes in naturally fractured reservoirs. Proc SPE Improved Oil Recov Symp Soc Petrol Eng. https://doi.org/10.2118/154246-MS

Neuman SP (2005) Trends, prospects and challenges in quantifying flow and transport through fractured rocks. Hydrogeol J 13(1):124–147. https://doi.org/10.1007/s10040-004-0397-2

Norbeck JH, Mcclure MW, Lo JW, Horne RN (2015) An embedded fracture modeling framework for simulation of hydraulic fracturing and shear stimulation. Comput Geosci 20(1):1–18. https://doi.org/10.1007/s10596-015-9543-2

Shakiba M (2014) Modeling and simulation of fluid flow in naturally and hydraulically fractured reservoirs using embedded discrete fracture model (EDFM). MS Thesis, University of Texas at Austin, Texas

Sun WJ, Wu Q, Liu HL, Jiao J (2015) Prediction and assessment of the disturbances of the coal mining in Kailuan to karst groundwater system. Phys Chem Earth Parts A/b/c 89:136–144. https://doi.org/10.1016/j.pce.2015.10.008

Timms WA, Crane R, Anderson DJ, Bouzalakos S, Whelan M, McGeeney D, Rahman F, Guinea A, Acworth RI (2014) Vertical hydraulic conductivity of a clayey-silt aquitard: accelerated fluid flow in a centrifuge permeameter compared with in situ conditions. Hydrol Earth Syst Sci Disc 11(3):3155–3212. https://doi.org/10.5194/hessd-11-3155-2014,%202014

Tiwary RK, Dhar BB (1994) Environmental pollution from coal mining activities in Damodar River basin, India. Mine Water Environ 13:1–10

Wang L, Wei SP, Wang QJ (2008) Effect of coal exploitation on groundwater and vegetation in the Yushenfu coal mine. J China Coal Soc 33(12):1408–1414 (**(in Chinese)**)

Wang G, Wu MM, Wang R, Xu H, Song X (2017) Height of the mining-induced fractured zone above a coal face. Eng Geol 216:140–152. https://doi.org/10.1016/j.enggeo.2016.11.024

Wu Q, Wang M (2006) Characterization of water bursting and discharge into underground mines with multilayered groundwater flow systems in the north China coal basin. Hydrogeol J 14(6):882–893. https://doi.org/10.1007/s10040-006-0021-8

Wu Q, Liu Y, Liu D, Zhou W (2011) Prediction of floor water inrush: the application of GIS-based AHP vulnerable index method to Donghuantuo coal mine. China Rock Mech Rock Eng 44(5):591. https://doi.org/10.1007/s00603-011-0146-5

Yihdego Y, Paffard A (2017) Predicting open pit mine inflow and recovery depth in the Durvuljin soum, Zavkhan Province. Mongolia Mine Water Environ 36(1):114–123. https://doi.org/10.1007/s10230-016-0419-z

Yin HY, Wei JC, Lefticariu L, Guo JB, Xie DL, Li ZL, Zhao P (2016) Numerical simulation of water flow from the coal seam floor in a deep longwall mine in China. Mine Water Environ 35(2):243–252. https://doi.org/10.1007/s10230-016-0385-5

Yin HY, Shi YL, Niu HG, Xie DL, Wei JC, Lefticariu L, Xu SX (2018) A GIS-based model of potential groundwater yield zonation for a sandstone aquifer in the Juye Coalfield, Shangdong, China. J Hydrol 557:434–447. https://doi.org/10.1016/j.jhydrol.2017.12.043

Yin HY, Sang SZ, Xie DL, ZhaoH LSJ, Li HS, Zhuang XH (2019) A numerical simulation technique to study fault activation characteristics during mining between fault bundles. Environ Earth Sci 78(5):148. https://doi.org/10.1007/s12665-019-8142-2

Yoon H, Jun SC, Hyun Y, Bae GO, Lee KK (2011) A comparative study of artificial neural networks and support vector machines for predicting groundwater levels in a coastal aquifer. J Hydrol 396(1–2):128–138. https://doi.org/10.1016/j.jhydrol.2010.11.002

Zawadzki J, Przeździecki K, Miatkowski Z (2016) Determining the area of influence of depression cone in the vicinity of lignite mine by means of triangle method and LANDSAT TM/ETM+ satellite images. J Environ Manag 166:605–614. https://doi.org/10.1016/j.jenvman.2015.11.010

Zhang J (2005) Investigations of water inrushes from aquifers under coal seams. Int J Rock Mech Min 42(3):350–360. https://doi.org/10.1016/j.ijrmms.2004.11.010

Zhang SZ, Guo WJ, Li YY (2017) Experimental simulation of water-inrush disaster from the floor of mine and its mechanism investigation. Arab J Geosci 10(22):503. https://doi.org/10.1007/s12517-017-3287-3

Zhou Q, Herrera J, Hidalgo A (2018) The numerical analysis of fault-induced mine water inrush using the extended finite element method and fracture mechanics. Mine Water Environ 37:185–195. https://doi.org/10.1007/s10230-017-0461-5

Zhu WC, Wei CH (2011) Numerical simulation on mining-induced water inrushes related to geologic structures using a damage-based hydromechanical model. Environ Earth Sci 62(1):43–54. https://doi.org/10.1007/s12665-010-0494-6